Electronic Supplementary Material (ESI) for Materials Horizons.
This journal is © The Royal Society of Chemistry 2022

Chemicals

1,3,5-triformylphloroglucinol (TFP, >98.0%) and 2,6-diaminoanthraquinone (DAAQ, >97.0%) were obtained from Tokyo Chemical Industry. Acetic acid (≥99.0%), ethanol (≥99.5%), and *N*,*N*-dimethylformamide (DMF, >99.5%) were purchased from Wako Pure Chemical Corporation. Poly(vinylidene fluoride) (PVDF 6020), *N*-methyl pyrrolidone (NMP, 99.5%), and carbon black (Super P) were bought from Sigma-Aldrich. All chemicals were used without further purification.

Synthetic procedures

Synthesis of DAAQ-functionalized MXene-NH_2. $Ti_3C_2T_x$ MXene was generated by the selective removal of Al interlayers from the original Ti_3AlC_2 MAX phase using aqueous solutions of LiF/HCl, followed by organic-solvent-intercalation-assisted ultrasonic exfoliation in N_2-saturated deionized water to prevent the oxidation of the MXene.[S1] To obtain the DAAQ-functionalized MXene-NH_2, 10.0 mg of freshly synthesized $Ti_3C_2T_x$ MXene was dispersed in ethanol (20 mL) and sonicated for 30 min; next 20 mL of DAAQ monomer (0.15 mM, DMF) and 1.5 mL of acetic acid (6 M) were added. The mixture was sonicated for 10 min and then heated at 90 °C for 1 h. The product was collected, washed several times with DMF and ethanol, and held for later use.

Synthesis of the MXene@COF heterostructure. In a typical synthesis of the MXene@COF heterostructure, 20.0 mg of the MXene-NH_2 precursor described above was ultrasonically dispersed in 20 mL of ethanol for 1 h to obtain a homogeneous solution. The TFP monomer (0.1 mM, 20 mL DMF) was added to this solution and stirred for 10 min; after which the DAAQ monomer (0.15 mM, 20 mL DMF) and 3 mL of HAc (6 M) were added, and the mixture was stirred for 30 min. Next, the mixture solution was heated at 90 °C for 24 h to assemble DAAQ-TFP-COF nanofibers on the surface of MXene-NH_2. The resultant precipitate, the MXene@COF heterostructure with a sandwich-like architecture, was finally collected via centrifugation and washed separately with DMF and ethanol several times. The supernatant was frozen in liquid nitrogen for 5 min and then transferred to a freeze drying machine (the pressure in the vacuum pump was $<1 \times 10^{-3}$ atm) at -85 °C for 24 h. The as-prepared MXene@COF heterostructure was fully dried, placed in capped glass vials, and stored under ambient conditions for further experiments.

Synthesis of heterostructures with different COF content. The MXene@COF heterostructures with different COF thicknesses were prepared; they are labeled MXene@COF-low and MXene@COF-high. The MXene@COF-low sample had a lower concentration of DAAQ-TFP-COF, or fewer COF nanofibers on the surfaces of the MXene nanosheets, than the previously described MXene@COF heterostructure, whereas the MXene@COF-high sample had a higher concentration of DAAQ-TFP-COF, or more COF nanofibers. The synthetic processes of MXene@COF-low and MXene@COF-high are similar to those of the MXene@COF

heterostructure. To obtain MXene@COF-low, 20 mL of TFP (0.02 mM, DMF) and 20 mL of DAAQ (0.03 mM, DMF) were added to the reaction system, whereas for MXene@COF-high, 20 mL of TFP (0.2 mM, DMF) and 20 mL of DAAQ (0.3 mM, DMF) were added to the reaction system.

Synthesis of pure DAAQ-TFP-COF. In a typical synthesis of pure DAAQ-TFP-COF,[S2,S3] 20 mL of DAAQ monomer (0.15 mM) was added to the DMF solution of TFP monomer (0.1 mM), followed by the addition of 3.0 mL HAc (6 M) and subsequent stirring for 30 min. Next, the mixture solution was heated at 90 °C for 24 h to promote the growth of pure DAAQ-TFP-COF. Pure DAAQ-TFP-COF was obtained via centrifugation, washed separately with DMF and ethanol several times, and then freeze-dried.

Synthesis of the MXene/COF hybrid. To directly synthesize the hybrid MXene/COF composite, denoted as the MXene/COF hybrid, 10.0 mg of freshly synthesized $Ti_3C_2T_x$ MXene was dispersed in 20 mL of ethanol and sonicated for 30 min; then the following mixture solution was added: DAAQ monomer (0.15 mM, 20 mL DMF), TFP monomer (0.1 mM, 20 mL DMF), and 3.0 mL of acetic acid (6 M). The mixture were stirred for 30 min and then heated at 90 °C for 24 h. Next, the MXene/COF hybrid was harvested via centrifugation, washed several times with DMF and ethanol, and freeze-dried.

Synthesis of MXene/COF mixture. To demonstrate the advantages of the MXene@COF heterostructure, a physical mixture of MXene and COFs, denoted as the MXene/COF mixture, was prepared directly by physically mixing MXene and DAAQ-TFP-COF; 10.0 mg of freshly synthesized $Ti_3C_2T_x$ MXene was dispersed in 20 mL of ethanol and sonicated for 30 min, after which 10 mg of DAAQ-TFP-COF was added. The mixture was stirred for 2 h and then washed several times with ethanol.

Characterization

The morphology of the as-synthesized materials was observed using field emission scanning electron microscopy (FESEM, Hitachi SU-8000) at an accelerating voltage of 10.0 kV. Transmission electron microscopy (TEM), scanning transmission electron microscopy (STEM), energy-dispersive X-ray spectroscopy (EDXS), and elemental mapping analysis were performed using a JEM-2100F instrument (JEOL, Japan) operated at 200 kV. Wide-angle X-ray diffraction (XRD) patterns were obtained using a Rigaku Rint 2000 X-ray diffractometer with monochromatic Cu Kα radiation (40 kV, 40 mA) at a scan rate of 2 °C min^{-1}. X-ray photoelectron spectroscopy (XPS) spectra were collected on a PHI Quantera SXM (ULVAC-PHI) instrument using Al Kα radiation, and the binding energies were calibrated by referencing them to the C 1s (284.5 eV) binding energy. Nitrogen (N_2) adsorption-desorption isotherms were obtained using a Quantachrome Autosorb-iQ automated gas sorption system at 77 K. The specific surface area was evaluated using the multipoint Brunauer-Emmett-Teller (BET) method at relative pressures ranging from 0.05 to 0.5 on the basis of the adsorption data. The pore size distributions were calculated from the adsorption branches of

the isotherms using a nonlocal density functional theory (DFT) method. The concentration of the NaCl solution was continuously measured by a REX DDSJ-308F conductivity meter (INESA Scientific Instrument, Shanghai, China).

Electrochemical measurements

To investigate the electrochemical performance of the MXene@COF heterostructure, cyclic voltammetry (CV) and galvanostatic charge/discharge (GCD) tests were conducted in a 1 M NaCl solution under an open air environment on a CHI 760E electrochemical workstation (Chenhua, Shanghai, China) in a three-electrode setup (a platinum counter electrode and a KCl-saturated Ag/AgCl reference electrode). To prepare the working electrodes (mass loading: 1 mg cm^{-2}), a homogeneous slurry of the MXene@COF heterostructure, PVDF, and carbon black at a mass ratio of 8: 1: 1 in NMP solvent was coated onto graphite paper and dried at 120 °C in a vacuum oven overnight.

The specific capacity (C) was calculated from the GCD curves based on discharge branch as follows:

$$C = I \times t \qquad \text{(S-1)}$$

where I (mA g^{-1}) is the specific current, and t (s) is the discharge time.

Capacitive deionization tests

MXene@COF heterostructure cathodes for capacitive deionization (CDI) were prepared as follows: MXene@COF, carbon black, and PVDF at a weight ratio of 8: 1: 1 were mixed in NMP solvent to form a slurry. The obtained slurry was coated on graphite paper (2 × 2 cm^2) to make cathodes. Active carbon (AC) anodes were fabricated by adjusting the mass of AC, carbon black, and PVDF to an 8: 1: 1 weight ratio in NMP and depositing the mixture on another piece of graphite paper (2 × 2 cm^2). Both the MXene@COF heterostructure cathodes and AC anodes with a mass loading of 2 mg cm^{-2} were dried at 120 °C in a vacuum drying oven overnight.

Desalination experiments were conducted in a batch-mode CDI testing system (that contains one pair of electrodes with anion and cation exchange membranes attached to the anode and cathode, respectively) in saline water containing dissolved oxygen, where the flow of O_2 was maintained over the whole duration of the CDI tests. Briefly, 32 mL of treating solution was continuously cycled by a peristaltic pump at a flow rate of 20 mL min^{-1} through the CDI device to a water reservoir, where a conductivity probe was installed. The solution conductivity was recorded by a conductivity meter every 30 s, and the real-time saline concentration was calculated from a linear calibration linear obtained before the experiments. The salt adsorption capacity (SAC, mg g^{-1}), areal SAC (mg cm^{-2}), mean salt adsorption rate at t min (MSAR, mg g^{-1} min^{-1}), and charge efficiency (Λ) were calculated as follows:

$$SAC = \frac{(C_0 - C_t) \times V}{m} \quad \text{(S-2)}$$

$$areal\ SAC = \frac{(C_0 - C_t) \times V}{S} \quad \text{(S-3)}$$

$$MSAR = \frac{SAC}{t} \quad \text{(S-4)}$$

$$\Lambda = \frac{SAC \times F \times m}{M \times 1000 \int_0^T i dt} \quad \text{(S-5)}$$

where C_0 and C_t are the NaCl concentrations at initial stage and t min (mg L^{-1}), respectively; V is the solution volume (L); m is the total mass of the active material on both the anode and cathode (g); S is the total surface area for both the anode and cathode (cm^2); F represents the Faraday constant (96 485 C mol^{-1}), M is the molar mass of NaCl (58.44 g mol^{-1}); T is the deionization time (s), and i is the recorded specific current (A g^{-1}).

Computational Method

The electronic structures were computed using DFT as implemented the Vienna ab initio Simulation package. The projector augmented wave model with the Perdew-Burke-Ernzerhof functional was employed to describe the interactions between the core and electrons. An energy cutoff of 450 eV was used for the planewave expansion of the electronic wave function. The Brillouin zones of all systems were sampled with gamma-point centered Monkhorst-Pack grids. Monkhorst-Pack *k*-point setups with sizes of 10 × 10 × 1 (1), 4× 2 × 1 (2 and 3) were used for slab geometry optimization. The force and energy convergence criteria were set to 0.02 eV $Å^{-1}$ and 10^{-5} eV, respectively.

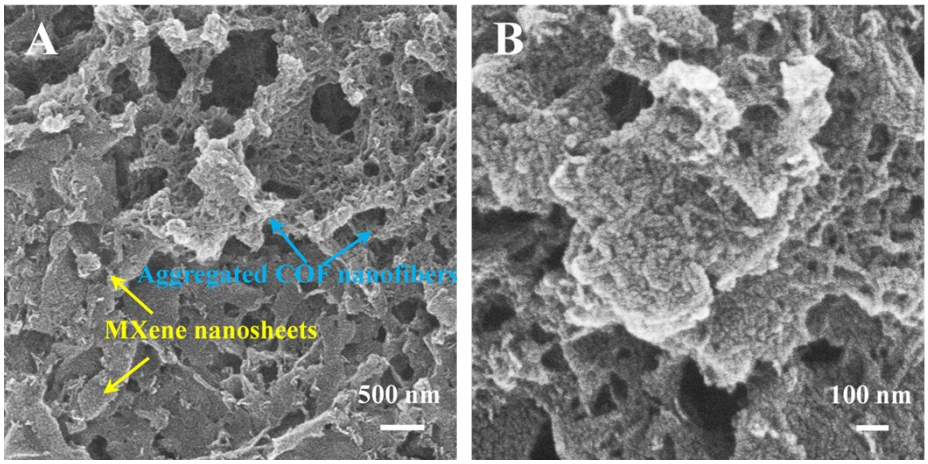

Fig. S1 SEM images of MXene/COF hybrid prepared by the direct growth of DAAQ-TFP-COF on MXene nanosheets without DAAQ modification.

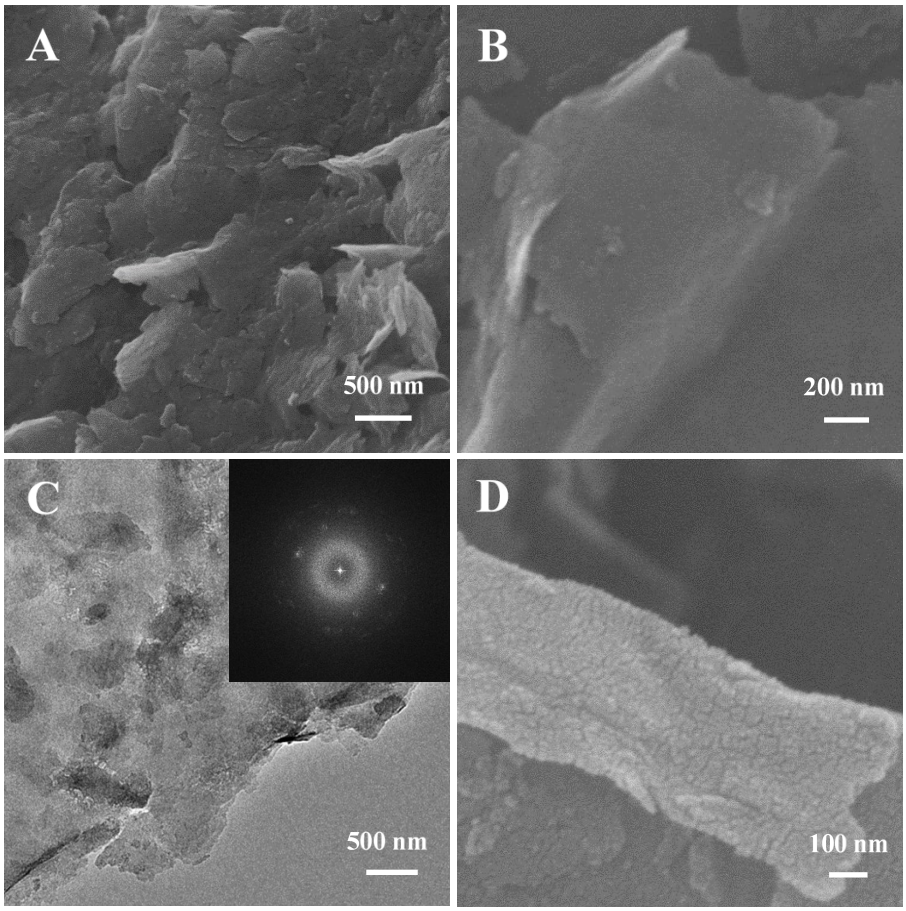

Fig. S2 (A, B) SEM images of pristine $Ti_3C_2T_x$ MXene nanosheets. (C) TEM image of $Ti_3C_2T_x$ MXene nanosheets (inset, SAED pattern). (D) SEM image of DAAQ-functionalized MXene-NH_2, which was obtained by linking of DAAQ monomer on MXene surface.

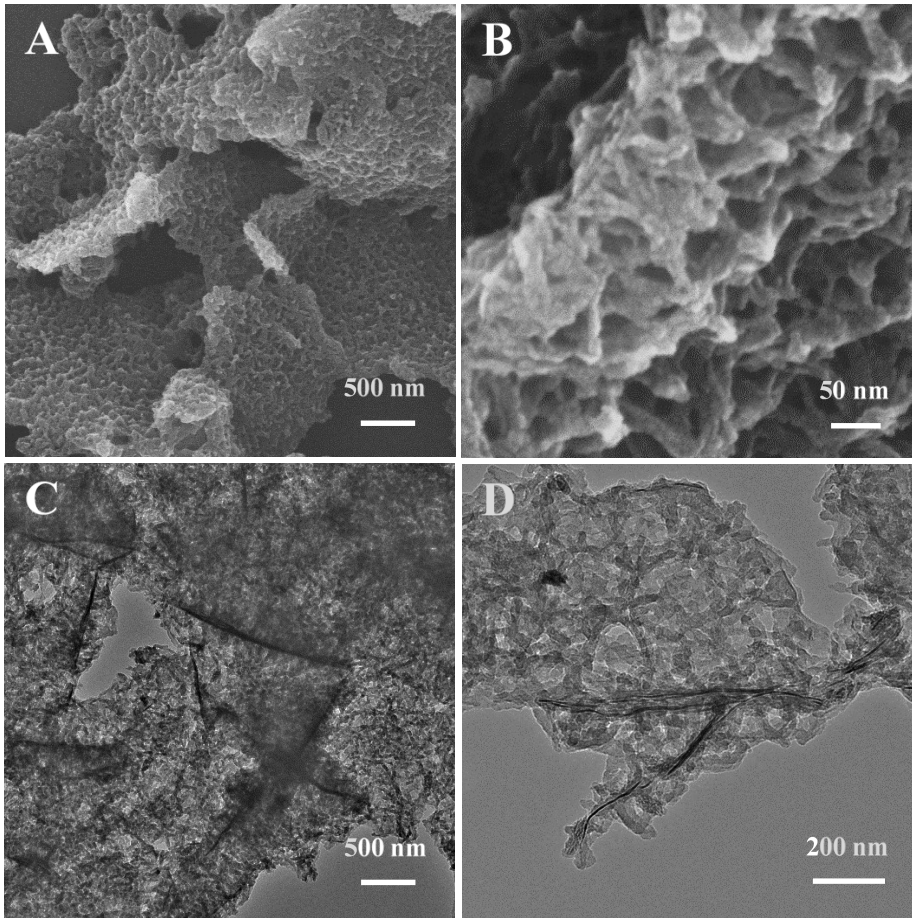

Fig. S3 Low- and high-resolution (A, B) SEM and (C, D) TEM images of MXene@COF heterostructure.

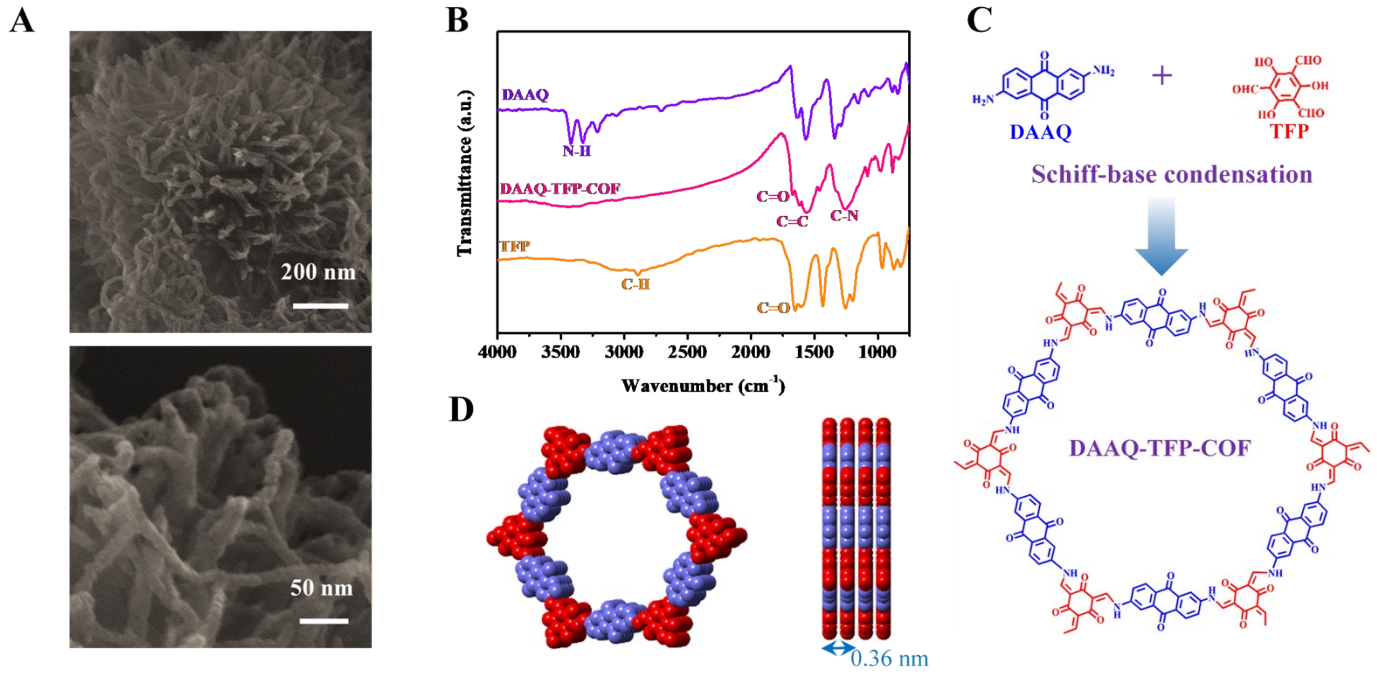

Fig. S4 (A) SEM images of pristine DAAQ-TFP-COF nanofibers. (B) FTIR spectra of DAAQ, TFP, and DAAQ-TFP-COF. (C) Schematic representation of DAAQ-TFP-COF synthesis. (D) Space-filling AA eclipsed stacking models of DAAQ-TFP-COF along the *c*- and *a*-axis directions.

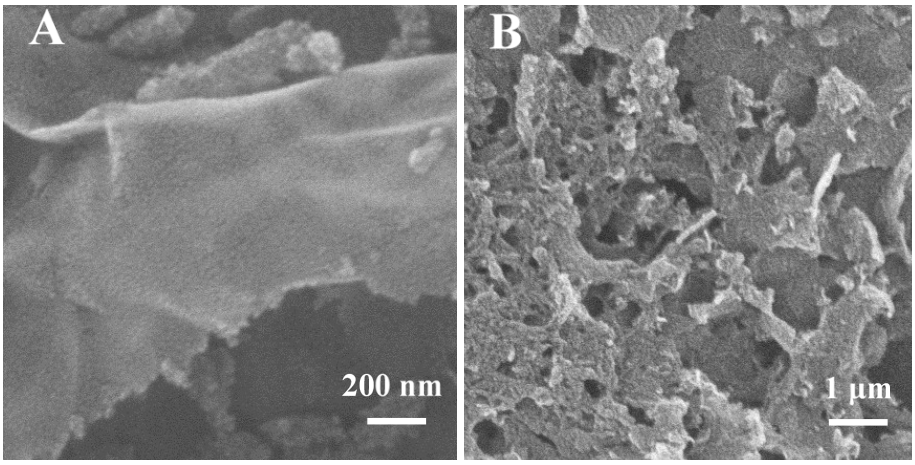

Fig. S5 SEM images of (A) MXene-NH_2-(0.03 mM) and (B) 0.03 mM DAAQ-MXene/COF.

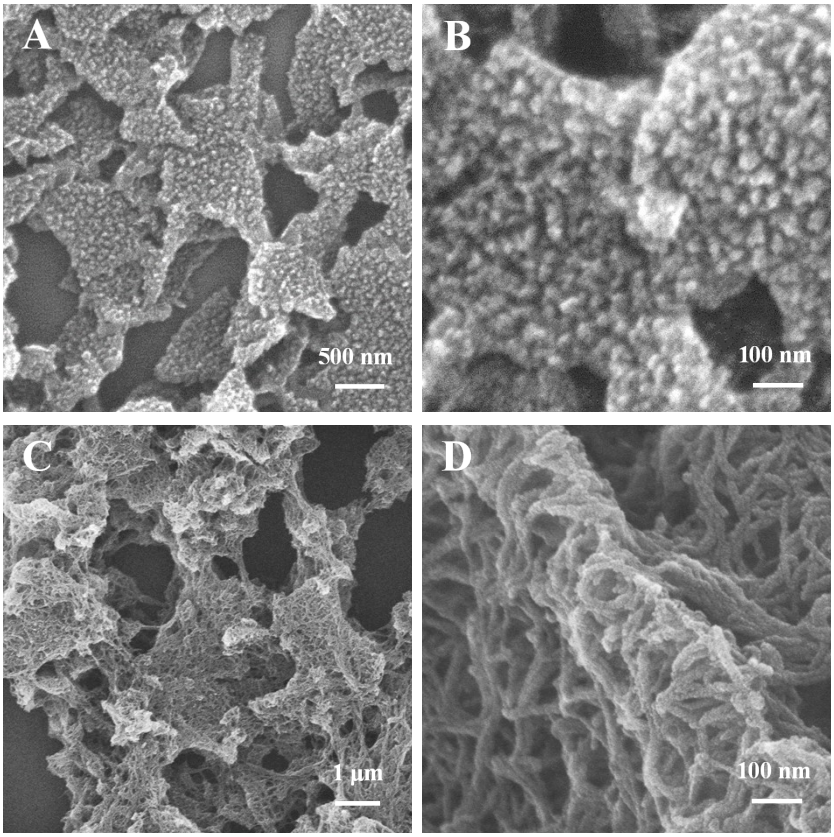

Fig. S6 SEM images of (A, B) MXene@COF-low and (C, D) MXene@COF-high. In MXene@COF-low (TFP, 0.02 mmoL; DAAQ, 0.03 mmoL), short oriented COF nanorods are uniformly deposited on the MXene surface (A, B), which may be attributed to the abundant nucleation sites on the MXene-NH_2 surface. In MXene@COF-high (TFP, 0.4 mmoL; DAAQ, 0.6 mmoL), excessive COF nanofibers are completely covered and overlap on the MXene-NH_2 nanosheets (C, D), and some COFs show an agglomerated morphology. However, no individual MXene nanosheets can be identified.

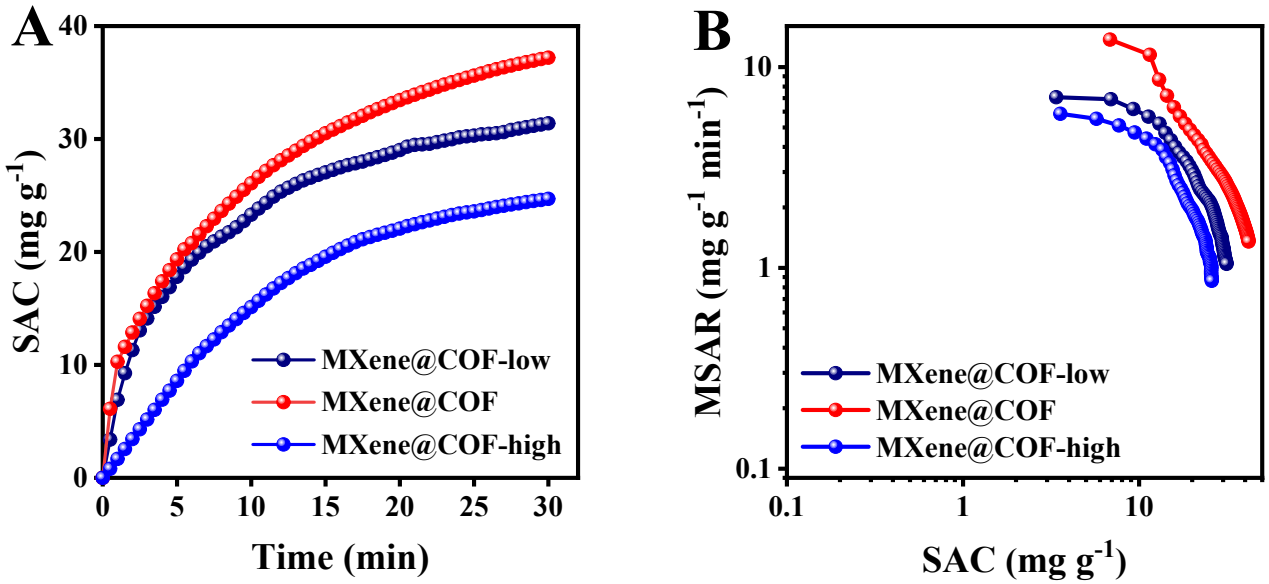

Fig. S7 (A) SAC curves and (B) corresponding CDI Ragone plots regarding to MSAR *versus* SAC of MXene@COF-low, MXene@COF, and MXene@COF-high.

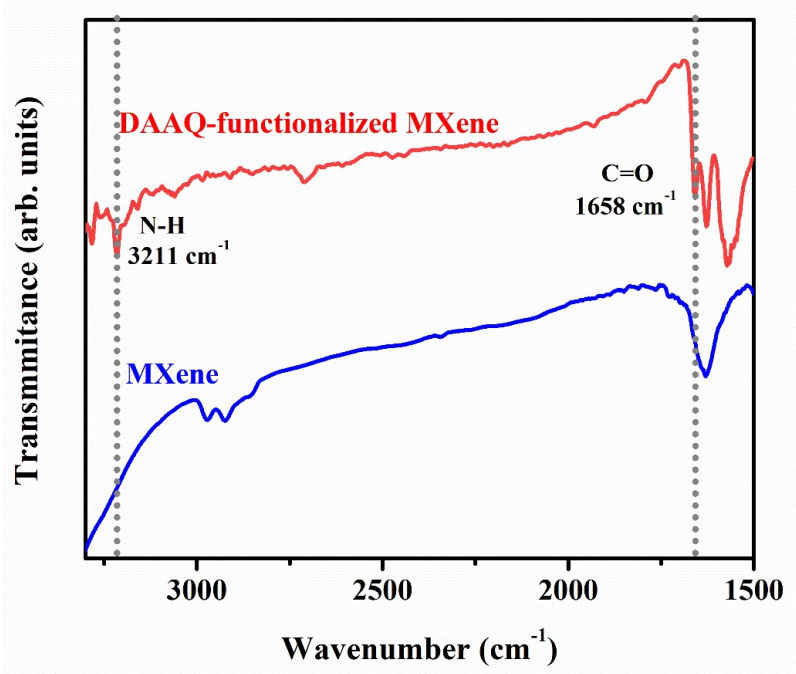

Fig. S8 FT-IR spectra of pristine MXene and DAAQ-functionalized MXene-NH_2 samples. As compared with the FT-IR spectrum of pristine MXene, the absorption peaks of DAAQ-functionalized MXene-NH_2 at 3211 and 1658 cm^{-1} were observed, suggesting the existence of -NH_2 and C=O groups on the surface of DAAQ-functionalized MXene-NH_2.

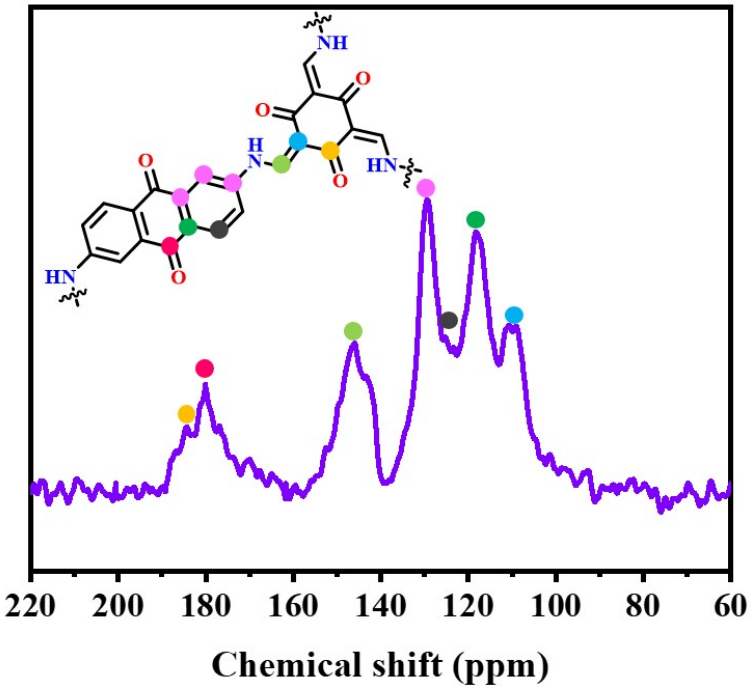

Fig. S9 Solid-state ^{13}C NMR spectrum of the MXene@COF heterostructure. The strong peak around 146 ppm can be ascribed to the enamine carbon atom (=C-NH-), confirming the successful formation of the *β*-ketoenamine-linked DAAQ-TFP-COF in the heterostructure.

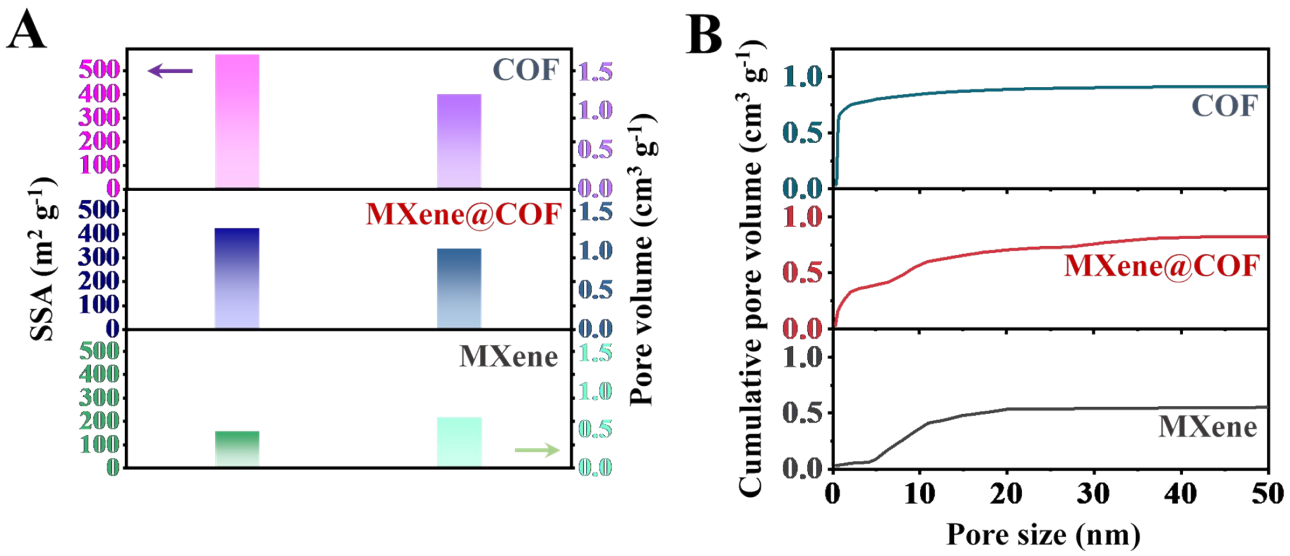

Fig. S10 (A) Specific surface area (SSA), pore volumes, and (B) cumulative pore size distributions of pure MXene, DAAQ-TFP-COF, and MXene@COF heterostructure.

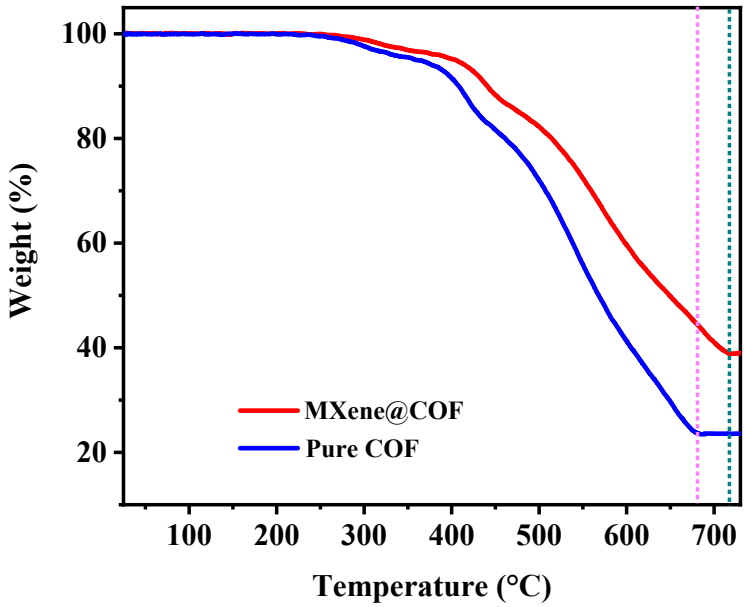

Fig. S11 TGA curves of pure COF and MXene@COF heterostructure from room temperature to 750 °C in N_2 atmosphere.

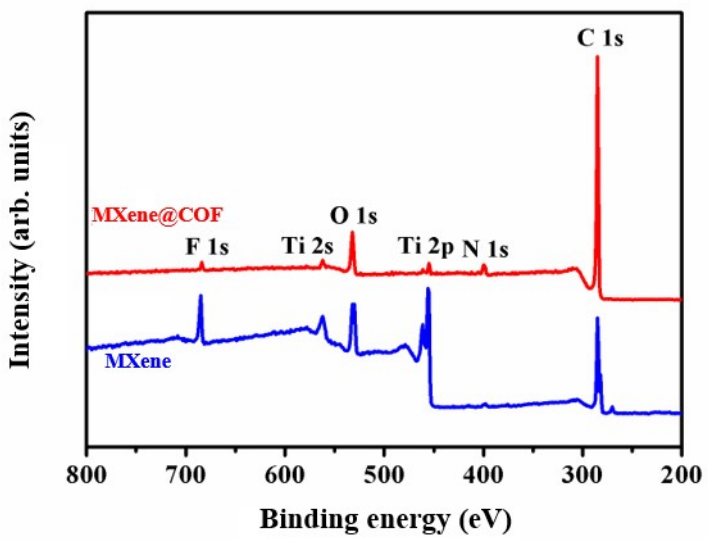

Fig. S12 XPS spectra of MXene and MXene@COF.

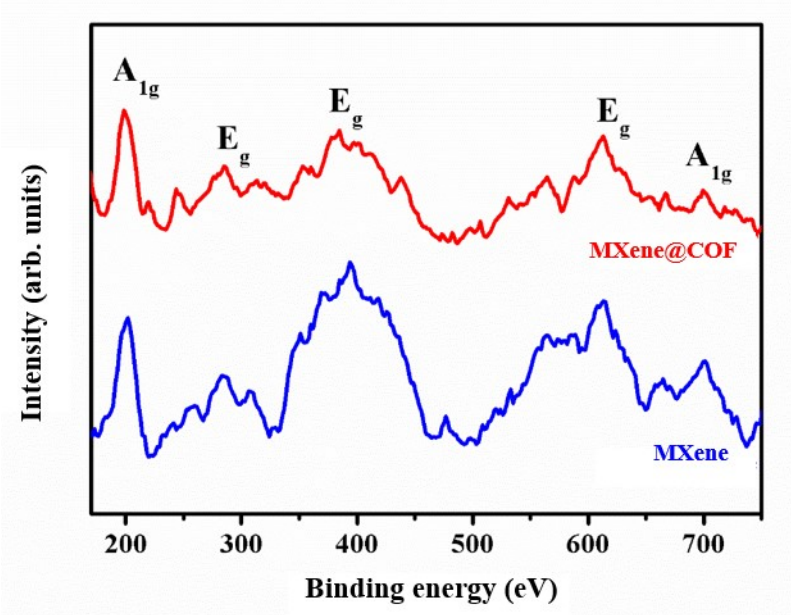

Fig. S13 Raman spectra of pure MXene and MXene@COF.

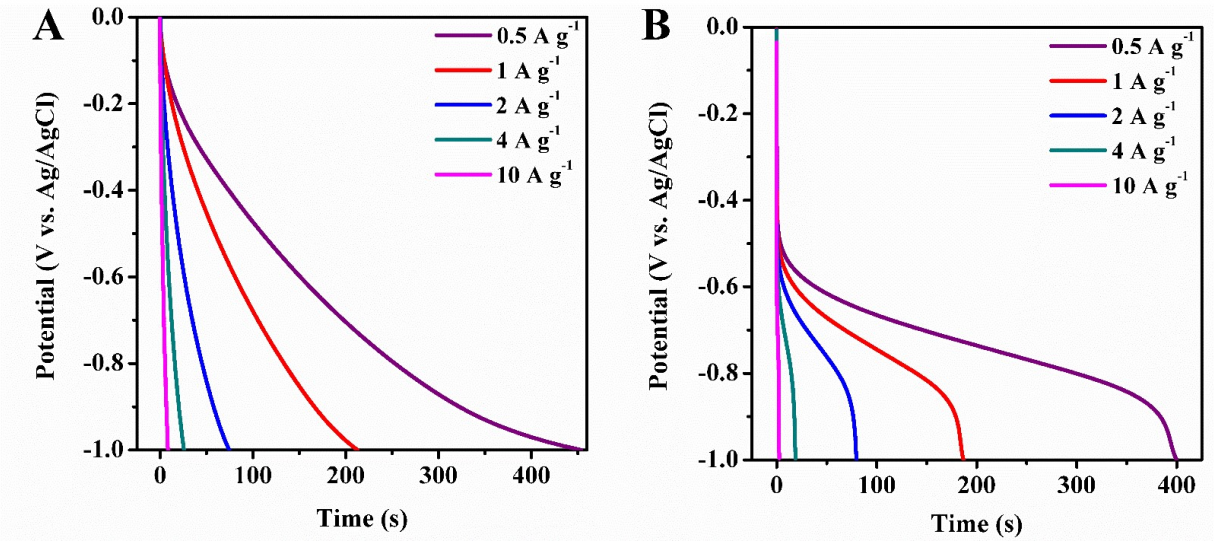

Fig. S14 Discharge curves of (A) pure MXene and (B) pure DAAQ-TFP-COF at current densities ranging from 0.5 to 10 A g^{-1}.

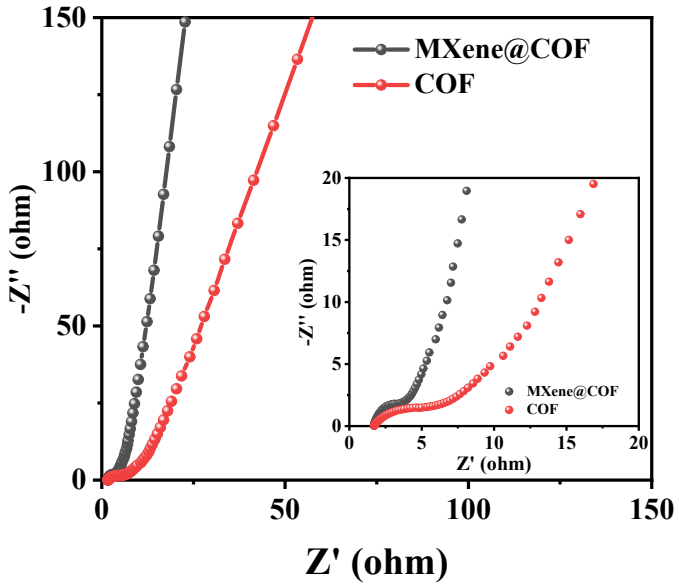

Fig. S15 Nyquist plots of the MXene@COF heterostructure and pure DAAQ-TFP-COF.

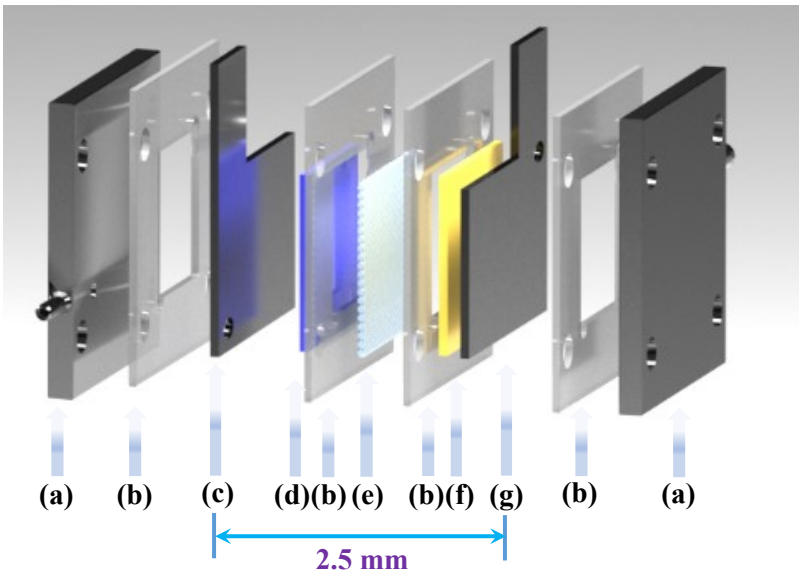

Fig. S16 The CDI device diagram with an MXene@COF as cathode and an AC anode. (a) Fastening plate; (b) Silicone gasket; (c) Cathode: graphite paper (2 × 2 cm^2) coated with 8 mg of MXene@COF (2 mg cm^{-2}); (d) Cation exchange membrane; (e) Non-woven fabrics spacer; (f) Anion exchange membrane; (g) Anode: graphite paper (2 × 2 cm^2) coated with 8 mg of AC (2 mg cm^{-2}).

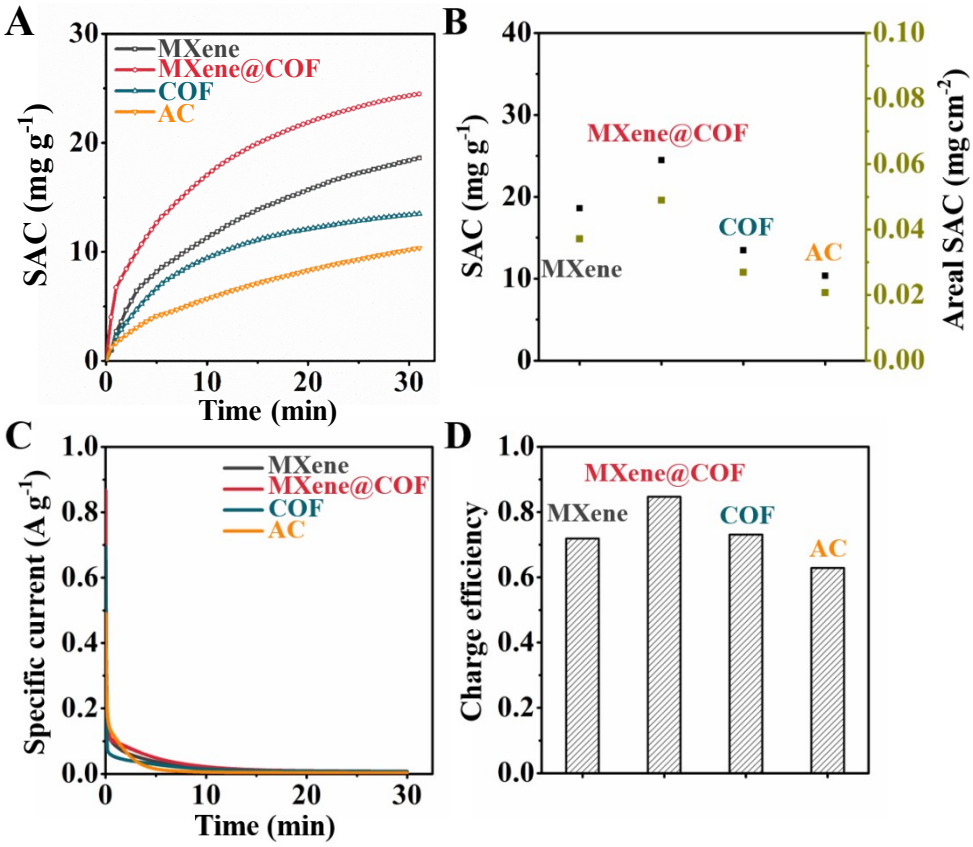

Fig. S17 (A) SAC *versus* time, (B) SAC and areal SAC values, (C) specific current *versus* time, and (D) charge efficiency for MXene, MXene@COF heterostructure, COF, and AC at 30 min (1.2 V, 500 mg L^{-1} NaCl solution).

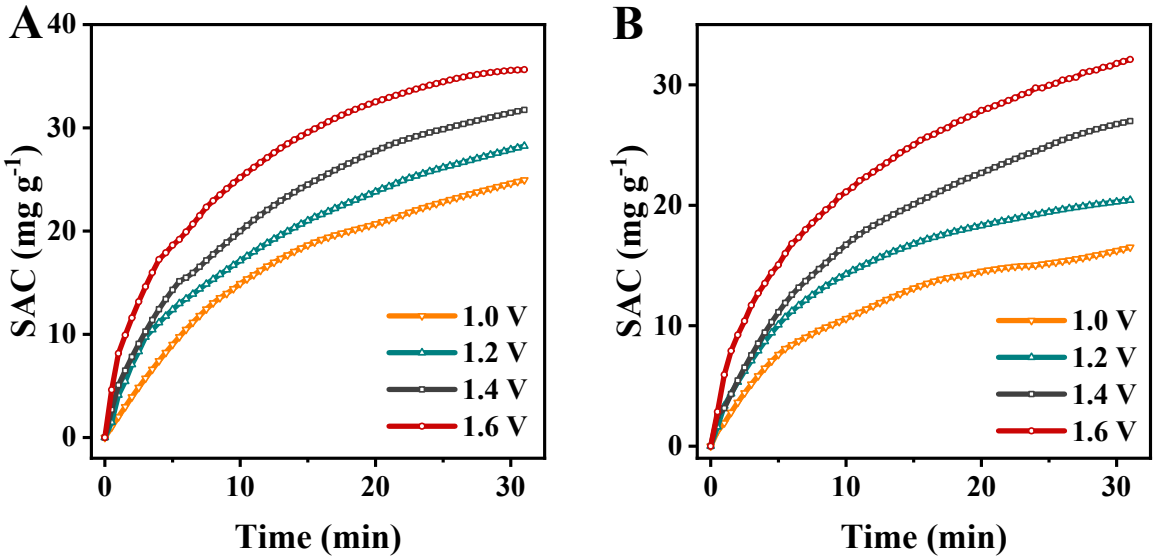

Fig. S18 SAC versus time for pure MXene (A) and pure COF (B) at operating voltages ranging from 1.0 to 1.6 V.

Table S1. CDI performance comparisons between MXene@COF and other faradic materials.

Electrode	Counter electrode	Voltage/V	SAC/mg g^{-1}	Ref.
MXene@COF	AC	1.6	53.1	This work
L-$Ti_3C_2T_x$ MXene	AC	1.2	30.08	S5
$Mo_{1.33}C$-MXene/CNT	Same	0.8	15	S6
MoS_2/MXene	AC	1.2	23.98	S7
Layered MnO_2	AC	1.2	37.2	S8
MnO_2	AC	1.4	14.9	S9
MnO_2	AC	1.4	34.15	S10
TiS_2/CNT	AC	0.8/0.2	14	S11
MoS_2	AC	0.8	25	S12
MoS_2/GO	AC	1.4	34.20	S13
N, S-doped $NaTi_2(PO_4)_3$/GO	AC	1.4	36.87	S14
MXene ($Ti_3C_2T_x$)	Same	1.2	13	S15
MXene-derived nitrogen doped fibers	AC	1.8	44.8	S16
Porous cryo-dried $Ti_3C_2T_x$	Same	1.2	45	S17
Ar plasma modification-MXene	AC	1.2	26.8	S18
MXene film	Same	1.2	11.9	S19
NaOH-$Ti_3C_2T_x$	AC	1.2	16.02	S20
LiF/HCl etched MXene	Same	1.2	67.7	S21
N doped-$Ti_3C_2T_x$	Same	1.2	43.5	S22
MXene-CNT	AC	1.2	9	S23
Cellulose fibers/MXene	Same	1.2	35	S24
MnO_2/ MWCNTs	AC	1.8	6.65	S25
Exfoliated MoS_2	Carbon textile	1.2	8.81	S26
Defect-rich MoS_2	CNT	0.8	24.6	S27
3D flower-like MoS_2/GO	AC	1.0	16.82	S28
MoS_2/PDA	Same	1.2	14.80	S29
MoS_2/Carbon	None	1.6	28.82	S30
MoS_2/AC	AC	1.2	8.98	S31

MoS_2/g-C_3N_4 composite	Same	1.6	24.2	S32
$NaTi_2(PO_4)_3$@C	AC	500 mA/g (0 ~ 2.0 V)	38.63*	S33
$NaTi_2(PO_4)_3$/C	AC	1.6	16.62*	S34
$NaTi_2(PO_4)_3$/MXene	AC	1.8	50.10*	S35
$Na_2FeP_2O_7$	AC	180 mA/g (-1.2 ~ 1.2 V)	30.2	S36
$VOHPO_4$/CNT	N.A.	50 mA/g (-0.1 ~ 0.4 V)	24.3	S37
$K_{0.03}Cu[Fe(CN)_6]_{0.65}\cdot 0.43H_2O$	AC	1.2	23.2	S38
NiHCF/rGO	rGO	0.6	22.8	S39
NiHCF	N.A.	0.4	34.0	S40
NiHCF@3DC-2	AC	1.2	47.8	S41
flowerlike PB	Same	1.0	31.6*	S42
$Na_4Mn_9O_{18}$	AC	1.2	31.2	S43
Carbon@$Na_4Ti_9O_{20}$	AC	1.4	66.14	S44
Graphene@$Na_4Ti_9O_{20}$	AC	1.0	26.74	S45
$Li_4Ti_5O_{12}$@carbon	AC	1.4	12	S46
$Na_{0.71}CoO_2$	Ag@rGO	1.0	20	S47
rGO/Co_3O_4	rGO	1.6	18.63	S48
Co_3O_4@CNF@CNT	CNF	1.2	42.0	S49
spinel $ZnCo_2O_4$	AC	1.2	39.4	S50
GO/ZrO_2	GO	1.2	6.3	S51
TiO_2/AC	AC	1.2	17	S52
TiO_2/CNTs	AC	1.2	4.3	S53
TiO_2/AC	AC	1.2	17.4	S54
Graphene aerogel/TiO_2	AC	1.2	15.1	S55
rGO/TiO_2 nanorod	AC	0.8	9.1	S56
MOF derived TiO_2@C	AC	10 mA/g (-1.4 ~ 1.4 V)	46.7	S57
TiO_2@COF	AC	1.6	33.66	S58
TiO_2/porous carbon	PC	1.2	38.54	S59
ACTN	AC	1.2	17.7	S60
ZnO/AC	AC	1.2	9.4	S61
ZnO-decorated AC	AC	1.2	3.93	S62

$Na_{0.44}MnO_2$	AgCl	100 mA/g (-1.4 ~ 1.4 V)	57.4	S63
2D-Fe_3O_4/C	AC	1.2	28.5	S64
3D rGO-Fe_2O_3	rGO	1.2	30.77	S65
α-MnO_2	AC	1.2	27.8	S66
α-MnO_2/graphene	graphene	1.2	29.5	S67
CNF@Mn_2O_3	CNF	1.2	27.43	S68
CNT/$NaMnO_2$	AC	1.2	32.7	S69
HC@MnO_2	HCs	1.2	30.7	S70
2D δ-MnO_2	AC	1.0	9.35	S71
MnO_2	AC-QPVP	1.4	14.9	S72
MnO_2@ACC	ACC	1.2	17.8	S73
MnO_2-nanorods@graphene	graphene	1.2	5.01	S74
MnO_x/CNT	ECNF	1.2	8.2	S75
ep-AC@MnO_2	N.A.	1.2	25.7	S76
Graphene-chitosan-Mn_3O_4	Graphene	1.6	12.7	S77
rGO-polypyrrole–MnO_2	RGO–PPy	2.0	18.4	S78
δ-MnO_2@Fe-CNF-5%	AC	1.1	20.0	S79
C-rGOMnPAN	rGO	1.0	6.0	S80
$MnFe_2O_4$/N-ACF	Same	1.2	36.9	S81
NM2-AC	AC	1.2	7.25	S82
MWCNT–hV_2O_5	AC	10 mA/g (-0.4 ~ 0.8 V)	23.6	S83
V_2O_5 nanocuboid	AC	30 mA/g (-0.6 ~ 1.2 V)	27.6*	S84
VO_xNTs/CNPT	AC	1.6	25	S85
$Na_{1.1}V_3O_{7.9}$@rGO	Ag@rGO	1.4	39.9	S86
RuO_2-AC	AC	1.2	11.26	S87
CuAl-LDO	AC	1.2	39.08	S88
CuAl-LDO/rGO	rGO-0.48	1.2	68	S89
N-TiO_{2-x}/C	AC	100 mA/g (-1.4 ~ 1.4 V)	33.4*	S90
Nb_2O_5@N–C-1	AC	1.2	35.4	S91
Graphene/SnO_2	Graphene	1.4	1.49	S92
SnO_2/PPAS-RGO	rGO	1.8	8.07	S93

$NiCo_4MnO_{8.5}$	Same	0.8	26.84	S94
4-MnO_2/HCS	HCS	1.2	30.86	S95
AC/ZnO	Same	1.2	3.93	S96
AC/Fe_2O_3	Same	1.2	6.76	S97
AC/Co_3O_4–Sb_2O_3–SnO_2	Same	1.2	23	S98
WS_2/rGO-CNT aerogel	rGO-CNT	10 mA/g (-1.4 ~ 1.4 V)	6.7	S99
SnS_2@GP	GP	1.2	30.32	S100
PPy-DBS/CNT	CNT	1.4	43.99	S101
CNT/PPy-DBS	CNT/PPy-Cl	1.2	36.12	S102
PPy-DBS/CNT	PPy-Cl/CNT	1.2	36.18	S103
Non-DR-GO/PPy	GO/PPy	1.2	26.60	S104
PNDIE	AC	1.8	45.9	S105
NCTs	NCTs	1.2	33	S106
$Na_2Ti_3O_7$-CNT@rGO	AC@rGO	145 mA/g (-1.4 ~ 1.4 V)	129	S107
$NaTi_2(PO_4)_3$/rGO	AC	100 mA/g (-1.4 ~ 1.4 V)	140	S108
$FePO_4$@rGO	AC	100 mA/g (-1.4 ~ 1.4 V)	100	S109
$FeFe(CN)_6$/rGA	rGA	100 mA/g (-1.4 ~ 1.4 V)	130	S110
Carbon fiber	NiCoAl-MMO	1.0 V	108.8	S111
PB/PANI	AC	100 mA/g (-1.4 ~ 1.4 V)	133	S112
PB@NPG	AC	125 mA/g (-1.4 ~ 1.4 V)	120	S113

*Note: Since the original SAC values in the corresponding papers were calculated based on dividing the mass of only single-side electrode, we corrected the values by dividing the mass of both-side electrodes in **Table S1**.

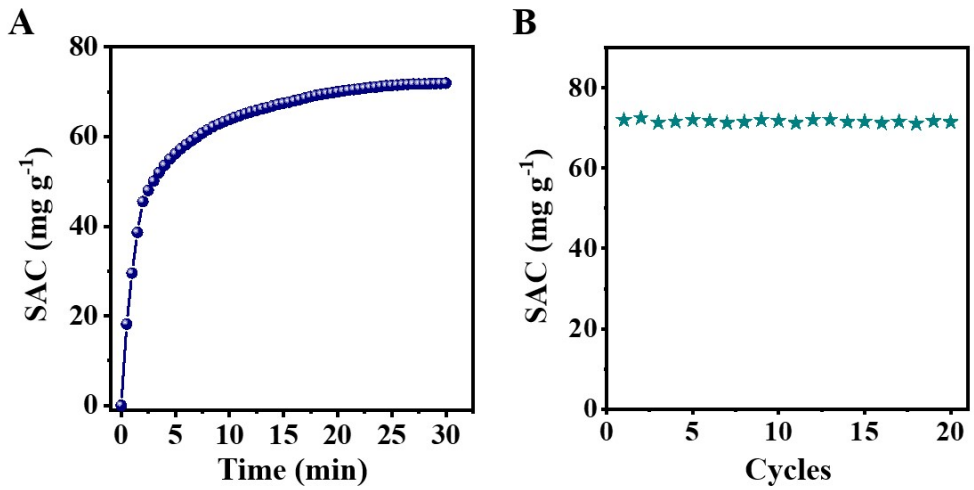

Fig. S19 (A) SAC *versus* time and (B) CDI cycling performance of the MXene@COF heterostructure in 600 mM NaCl solution.

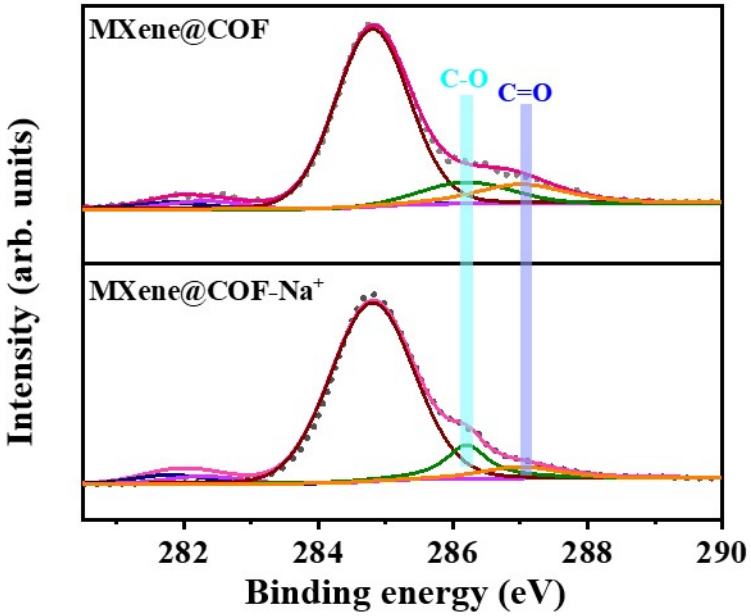

Fig. S20 *Ex-situ* XPS measurements of C 1*s* in MXene@COF and MXene@COF adsorbed with Na^+.

Note for Fig. S20. The MXene@COF heterostructure with the redox-active DAAQ groups showed a different XPS characterizations in C 1*s* core level spectra. In comparison with MXene@COF, the characteristic peak of C–O increases, but the C=O bond achieves a lower intensity, owing the quinone-to-hydroquinone tautomerism after the adsorption of Na^+ (also shown in **Scheme 1B**).[S2,S4] The change of C-O and C=O peaks in C 1*s* in MXene@COF further demonstrated the successful Na^+ incorporation into MXene@COF.

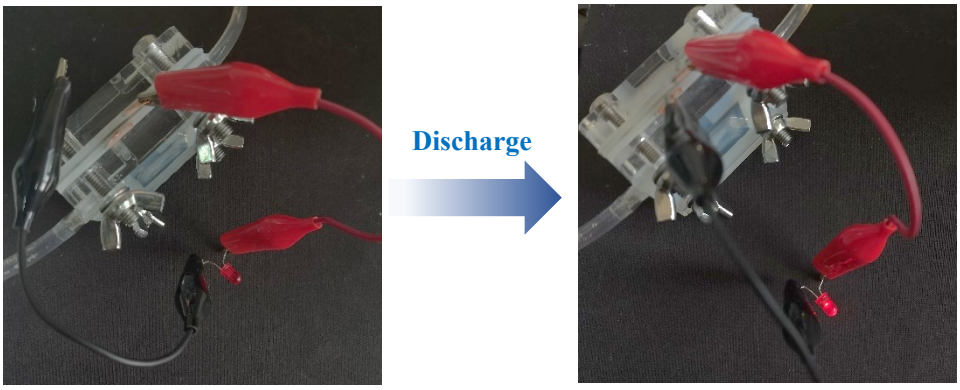

Fig. S21 Photographs for the MXene@COF heterostructure-based CDI serveing as a power source to drive an LED. The red light-emitting diode (LED) bulb was successfully illuminated by using the electricity recovered from the MXene@COF heterostructure-based CDI after the desalination process.

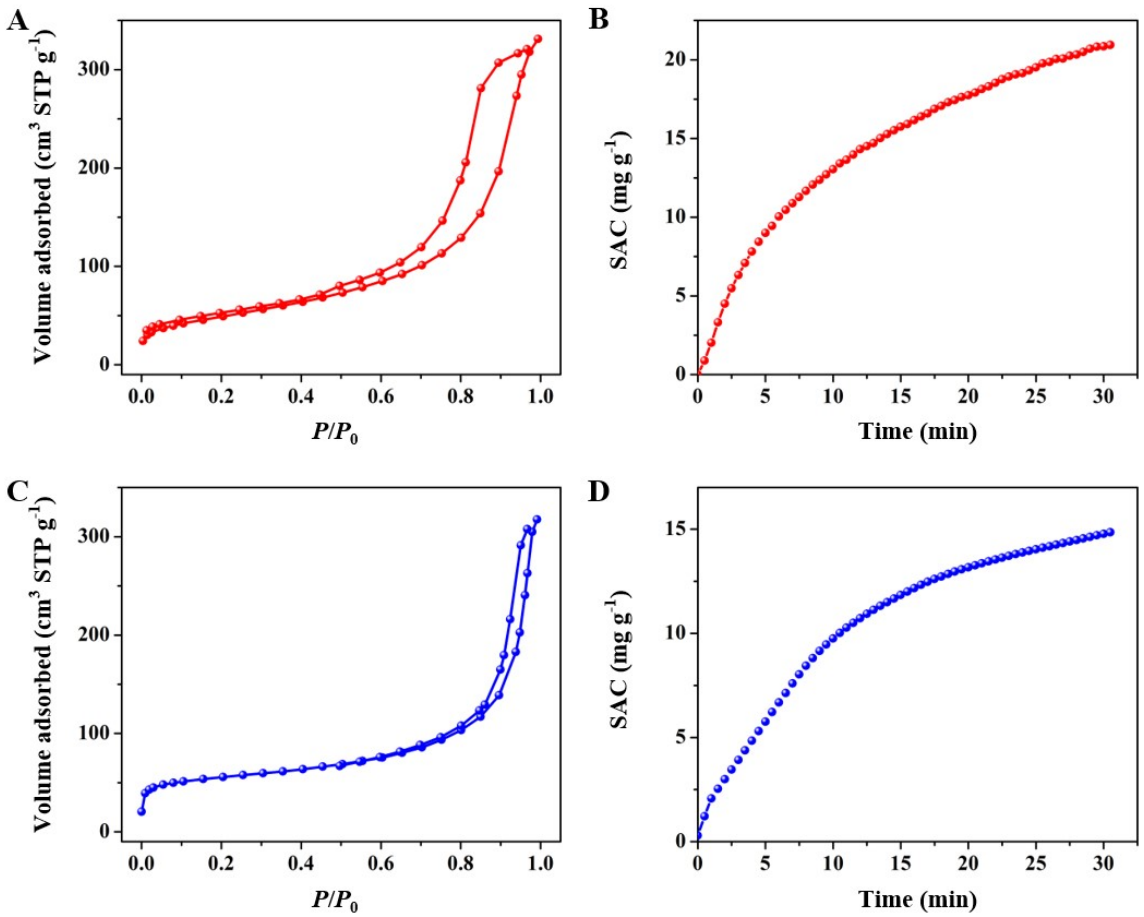

Fig. S22 (A, C) N_2 adsorption–desorption isotherms and (B, D) SAC *versus* time for (A, B) MXene/COF hybrid and (C, D) MXene/COF mixture.

Table S2. SSA, pore volume and SAC of MXene/COF hybrid and MXene/COF mixture at 1.2 V in 1000 mg L^{-1} NaCl solution.

Sample	SSA (m^2 g^{-1})	Pore volume (cm^3 g^{-1})	SAC (mg g^{-1})
MXene/COF hybrid	263	0.86	32.9
MXene/COF mixture	196	0.79	23.6

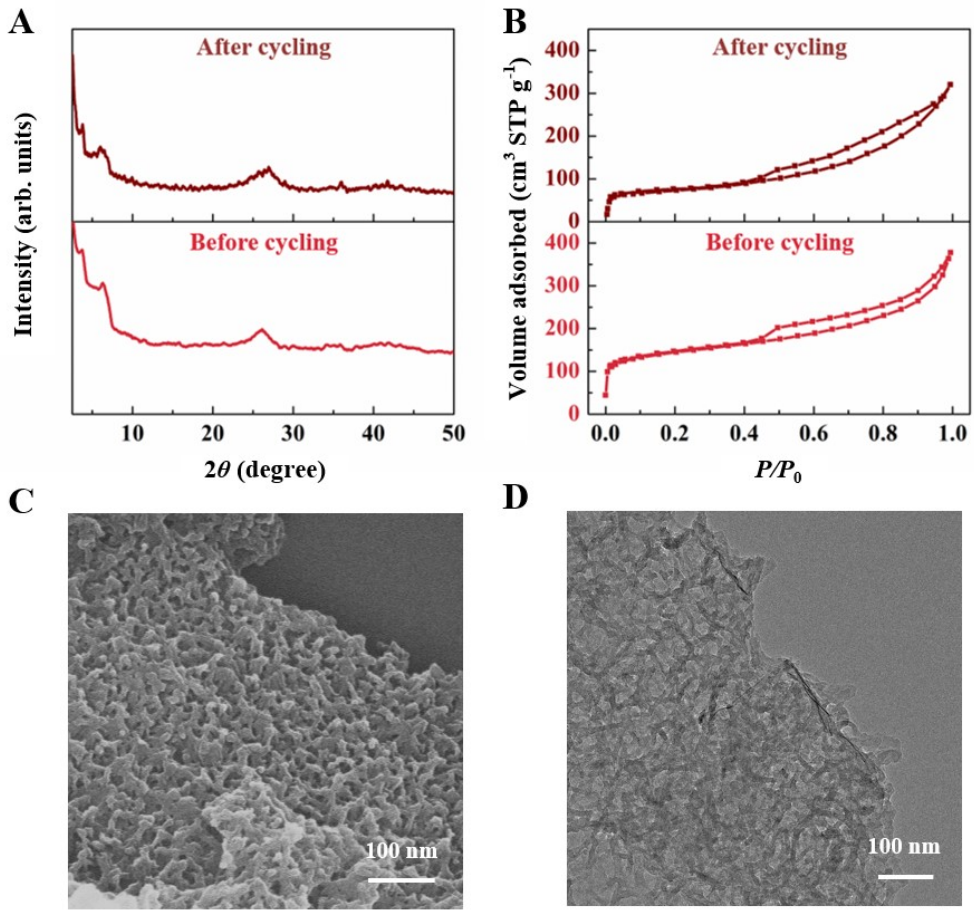

Fig. S23 (A) XRD patterns and (B) N_2 adsorption–desorption isotherms of MXene@COF heterostructure before use and after 100 CDI cycles. The surface area and the pore volume of MXene@COF heterostructure before use are 424 m^2 g^{-1} and 1.03 cm^3 g^{-1}, respectively, while those of MXene@COF heterostructure after 100 CDI cycles are 396 m^2 g^{-1} and 0.87 cm^3 g^{-1}, respectively. (C) SEM and (D) TEM images of the MXene@COF heterostructure after 100 CDI cycles.

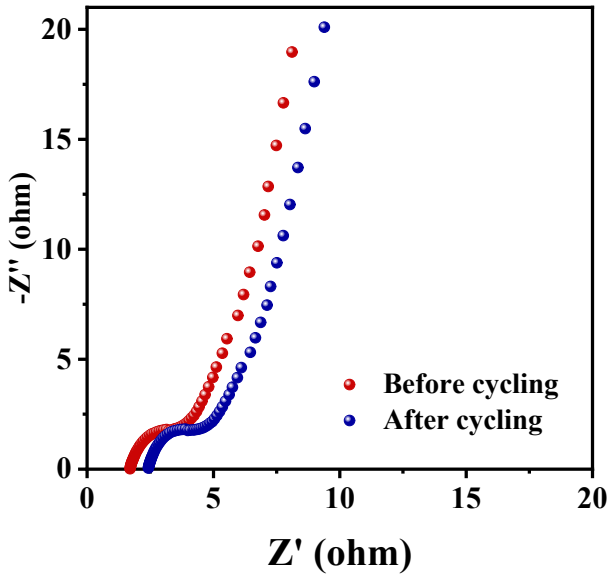

Fig. S24 Nyquist plots of the MXene@COF heterostructure before use and after 100 CDI cycles.

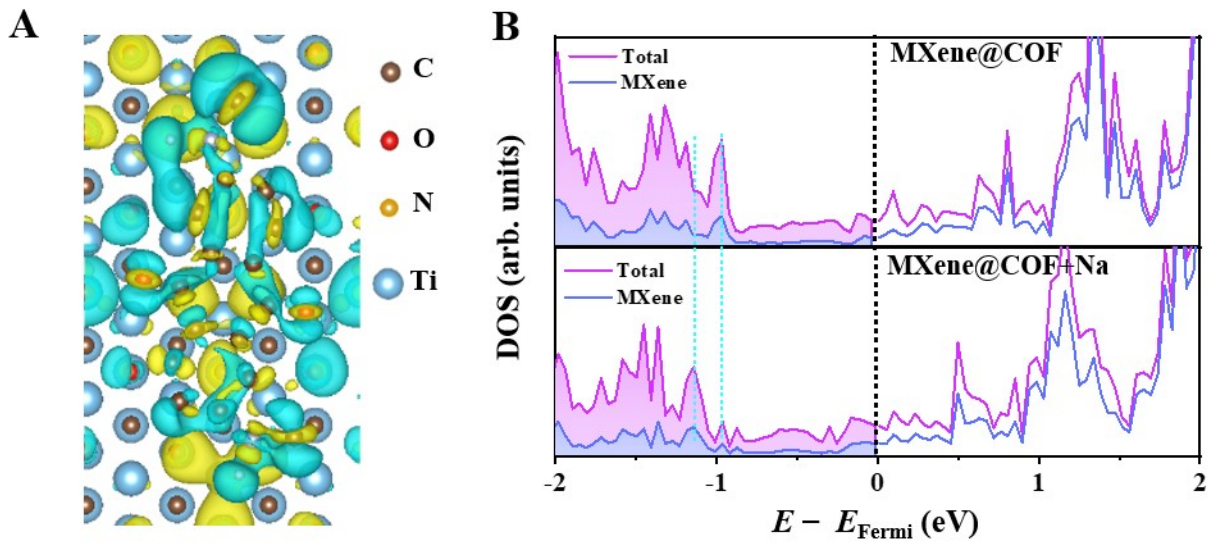

Fig. S25 (A) Electron density change at MXene@COF interface, where decreases and increases in electron density are indicated by green and yellow, respectively. (B) Electron density of states (DOS) of MXene and MXene@COF interface in the absence and presence of Na.

References

S1. M. R. Lukatskaya, S. Kota, Z. Lin, M. Q. Zhao, N. Shpigel, M. D. Levi, J. Halim, P.-L. M. W. Taberna, Barsoum, P. Simon and Y. Gogotsi, *Nat. Energy* 2017, **2**, 17105.

S2. C. R. DeBlase, K. E. Silberstein, T.-T. Truong, H. D. Abruña and W. R. Dichtel, *J. Am. Chem. Soc.* 2013, **135**, 16821-16824.

S3. C. R. DeBlase, K. Hernández-Burgos, K. E. Silberstein, G. G. Rodríguez-Calero, R. P. Bisbey, H. D.Abruña and W. R. Dichtel, *ACS Nano* 2015, **9**, 3178-3183.

S4. D. S. Achilleos and T. A. Hatton. *ACS Appl. Mater. Interfaces*, 2016, **8**, 32743-32753.

S5 S. Buczek, M. L. Barsoum, S. Uzun, N. Kurra, R. Andris, E. Pomerantseva, K. A. Mahmoud and Y. Gogotsi, *Energy Environ. Mater.* 2020, **3**, 398-404.

S6 P. Srimuk, J. Halim, J. Lee, Q. Tao, J. Rosen and V. Presser, *ACS Sustainable Chem. Eng.* 2018, **6**, 3739-3747.

S7 Z. Chen, X. Xu, Y. Liu, J. Li, K. Wang, Z. Ding, F. Meng, T. Lu and L. Pan, *Desalination* 2022, **528**, 115616.

S8 B. W. Byles, B. Hayes-Oberst and E. Pomerantseva, *ACS Appl. Mater. Interfaces* 2018, **10**, 32313-32322.

S9 T. Wu, G. Wang, S. Wang, F. Zhan, Y. Fu, H. Qiao and J. Qiu, *Environ. Sci. Technol. Lett.* 2018, **5**, 98-102.

S10 G. Tan, S. Lu, N. Xu, D. Gao and X. Zhu, *Environ. Sci. Technol.* 2020, **54**, 5843-5852.

S11 P. Srimuk, J. Lee, A. Tolosa, C. Kim, M. Aslan and V. Presser, *Chem. Mater.* 2017, **29**, 9964-9973.

S12 P. Srimuk, J. Lee, S. Fleischmann, S. Choudhury, N. Jaeckel, M. Zeiger, C. Kim, M. Aslan and V. Presser, *J. Mater. Chem. A* 2017, **5**, 15640-15649.

S13 L. Gao, Q. Dong, S. Bai, S. Liang, C. Hu and J. Qiu, *ACS Sustainable Chem. Eng.* 2020, **8**, 9690-9697.

S14 S. Liang, C. Han, Q. Meng, G. Tian and G. Y. Tian, *J. Mater. Sci.* 2020, **55**, 6017-6029.

S15 P. Srimuk, F. Kaasik, B. Krüner, A. Tolosa, S. Fleischmann, N. Jäckel, M. C. Tekeli, M. Aslan, M. E. Suss and V. Presser, *J. Mater. Chem. A* 2016, **4**, 18265-18271.

S16 Z. Ding, X. Xu, J. Li, Y. Li, K. Wang, T. Lu, M.S.A. Hossain, M. A. Amin, S. Zhang, L. Pan and Y. Yamauchi, *Chem. Eng. J.* 2022, **430**, 133161.

S17 W. Bao, T. Xiao, G. Xin, S. Choi and G. Wang, *Joule* 2018, **2**, 778-787.

S18 L. Guo, X. Wang, Z. Y. Leong, R. Mo, L. Sun and H. Y. Yang, *FlatChem* 2018, **8**, 17-24.

S19 L. Agartan, K. Hantanasirisakul, S. Buczek, B. Akuzum, K. A. Mahmoud, B. Anasori, Y. Gogotsi and E. C. Kumbur, *Desalination* 2020, **477**, 114267.

S20 B. Chen, A. Feng, R. Deng, K. Liu, Y. Yu and L. Song, *ACS Appl. Mater. Interfaces* 2020, **12**, 13750-13758.

S21 J. Ma, Y. Cheng, L. Wang, X. Dai and F. Yu, *Chem. Eng. J.* 2020, **384**, 123329.

S22 A. Amiri, Y. Chen, C. B. Teng and M. Naraghi, *Energy Storage Mater.* 2020, **25**, 731-739.

S23 M. Torkamanzadeh, L. Wang, Y. Zhang, Ö. Budak, P. Srimuk and V. Presser, *ACS Appl. Mater. Interfaces* 2020, **12**, 26013-26025.

S24 S. Anwer, D. H. Anjum, S. Luo, Y. Abbas, B. Li, S. Iqbal and K. Liao, *Chem. Eng. J.* 2021, **406**, 126827.

S25 B. Chen, Y. Wang, Z. Chang, X. Wang, M. Li, X. Liu, L. Zhang and Y. Wu, *RSC Adv.* 2016, **6**, 6730-6736.

S26 F. Xing, T. Li, J. Li, H. Zhu, N. Wang and X. Cao, *Nano Energy* 2017, **31**, 590-595.

S27 J. Han, T. Yan, J. Shen, L. Shi, J. Zhang and D. Zhang, *Environ. Sci. Technol.* 2019, **53**, 12668-12676.

S28 W. Peng, W. Wang, G. Han, Y. Huang and Y. Zhang, *Desalination* 2020, **473**, 114191.

S29 Q. Wang, F. Jia, S. Song and Y. Li, *Sep. Purif. Technol.* 2020, **236**, 116298.

S30 S. Tian, X. Zhang and Z. Zhang, *Chem. Eng. J.* 2021, **409**, 128200.

S31 B. Pan, Y. Q. Wang, H. B. Li, W. Yi and Y. Pan, *Int. J. Electrochem. Sci.* 2020, **15**, 1861-1880.

S32 S. Tian, X. Zhang and Z. Zhang, *Desalination* 2020, **479**, 114348.

S33 Z. Guo, Y. Ma, X. Dong, M. Hou, Y. Wang and Y. Xia, *ChemSusChem*, 2018, **11**, 1741-1745.

S34 K. Wang, Y. Liu, Z. Ding, Y. Li, T. Lu and L. Pan, *J. Mater. Chem. A*, 2019, **7**, 12126-12133.

S35 Z. Chen, X. Xu, Z. Ding, K. Wang, X. Sun, T. Lu, M. Konarova, M. Eguchi, J. G. Shapter, L. Pan and Y. Yamauchi, *Chem. Eng. J.*, 2021, **407**, 127148.

S36 S. Kim, J. Lee, C. Kim and J. Yoon, *Electrochim. Acta*, 2016, **203**, 265-271.

S37 J. Lee, P. Srimuk, R. Zwingelstein, R. L. Zornitta, J. Choi, C. Kim and V. Presser, *J. Mater. Chem. A*, 2019, **7**, 4175-4184.

S38 S. Choi, B. Chang, S. Kim, J. Lee, J. Yoon and J. W. Choi, *Adv. Funct. Mater.*, 2018, **28**, 1802665.

S39 Z. Ding, X. Xu, Y. Li, K. Wang, T. Lu and L. Pan, *Desalination*, 2019, **468**.

S40 S. Porada, A. Shrivastava, P. Bukowska, P. M. Biesheuvel and K. C. Smith, *Electrochim. Acta*, 2017, **255**, 369-378.

S41 S. Wang, G. Wang, Y. Wang, H. Song, S. Lv, T. Li and C. Li, *ACS Appl. Mater. Interfaces*, 2020, **12**, 44049-44057.

S42 A. Gong, Y. Zhao, X. Zhang, B. Liang, W. Zhang and K. Li, *Sep. Purif. Technol.*, 2022, **285**, 120333.

S43 J. Lee, S. Kim, C. Kim and J. Yoon, *Energy Environ. Sci.*, 2014, **7**, 3683-3689.

S44 Z. Yue, T. Gao and H. Li, *Desalination*, 2019, **449**, 69-77.

S45 F. Zhou, T. Gao, M. Luo and H. Li, *Chem. Eng. J.*, 2018, **343**, 8-15.

S46 L. Guo, D. Kong, M. E. Pam, S. Huang, M. Ding, Y. Shang, C. Gu, Y. Huang and H. Y. Yang, *J. Mater. Chem. A*, 2019, **7**, 8912-8921.

S47 Z. Liu, Z. Yue and H. Li, *Sep. Purif. Technol.*, 2020, **234**, 116090.

S48 G. Divyapriya, K. K. Vijayakumar and I. Nambi, *Desalination*, 2019, **451**, 102-110.

S49 L. Guo, J. Zhang, M. Ding, C. Gu, S. Vafakhah, W. Zhang, D.-S. Li, P. Valdivia y Alvarado and H. Y. Yang, *Sep. Purif. Technol.*, 2021, **266**, 118593.

S50 W. Si and H. Li, *Adv. Mater. Interfaces*, 2021, **8**, 2100125.

S51 A. S. Yasin, H. O. Mohamed, I. M. A. Mohamed, H. M. Mousa and N. A. M. Barakat, *Sep. Purif. Technol.*, 2016, **171**, 34-43.

S52 C. Kim, J. Lee, S. Kim and J. Yoon, *Desalination*, 2014, **342**, 70-74.

S53 H. Li, Y. Ma and R. Niu, *Sep. Purif. Technol.*, 2016, **171**, 93-100.

S54 P. Srimuk, M. Zeiger, N. Jäckel, A. Tolosa, B. Krüner, S. Fleischmann, I. Grobelsek, M. Aslan, B. Shvartsev, M. E. Suss and V. Presser, *Electrochim. Acta*, 2017, **224**, 314-328.

S55 H. Yin, S. Zhao, J. Wan, H. Tang, L. Chang, L. He, H. Zhao, Y. Gao and Z. Tang, *Adv. Mater.*, 2013, **25**, 6270-6276.

S56 A. G. El-Deen, J.-H. Choi, C. S. Kim, K. A. Khalil, A. A. Almajid and N. A. M. Barakat, *Desalination*, 2015, **361**, 53-64.

S57 M. Ding, S. Fan, S. Huang, M. E. Pam, L. Guo, Y. Shi and H. Y. Yang, *ACS Appl. Energ. Mater.*, 2019, **2**, 1812-1822.

S58 X. Liu, S. Zhang, G. Feng, Z.-G. Wu, D. Wang, M. D. Albaqami, B. Zhong, Y. Chen, X. Guo, X. Xu and Y. Yamauchi, *Chem. Mater.*, 2021, **33**, 1657-1666.

S59 L. Huang, T. Yan, A. E. D. Mahmoud, S. Li, J. Zhang, L. Shi and D. Zhang, *Environ. Sci.- Nano*, 2021, **8**, 950-959.

S60 A. G. El-Deen, J.-H. Choi, K. A. Khalil, A. A. Almajid and N. A. M. Barakat, *RSC Adv.*, 2014, **4**, 64634-64642.

S61 J. Liu, M. Lu, J. Yang, J. Cheng and W. Cai, *Electrochim. Acta*, 2015, **151**, 312-318.

S62 A. S. Yasin, D. h. Kim and K. Lee, *J. Alloy. Compd.*, 2021, **870**, 159422.

S63 F. Chen, Y. Huang, L. Guo, L. Sun, Y. Wang, H. Y. Yang, *Energy Environ. Sci.*, 2017, **10**, 2081.

S64 L. Chen, X. Xu, L. Wan, G. Zhu, Y. Li, T. Lu, M. D. Albaqami, L. Pan and Y. Yamauchi, *Mater. Chem. Front.*, 2021, **5**, 3480-3488.

S65 Y. Belaustegui, I. Rincón, F. Fernández-Carretero, P. Azpiroz, A. García-Luís and D. A. P. Tanaka, *Chem. Eng. J. Adv.*, 2021, **6**, 100094.

S66 B. W. Byles, D. A. Cullen, K. L. More and E. Pomerantseva, *Nano Energy*, 2018, **44**, 476-488.

S67 M. A. Jaoude, E. Alhseinat, K. Polychronopoulou, G. Bharath, I. F. F. Darawsheh, S. Anwer, M. A. Baker, S. J. Hinder and F. Banat, *Electrochim. Acta*, 2020, **330**, 135202.

S68 Y. Liu, X. Gao, L. Zhang, X. Shen, X. Du, X. Dou and X. Yuan, *Desalination*, 2020, **494**, 114665.

S69 S. Wang, G. Wang, X. Che, S. Wang, C. Li, D. Li, Y. Zhang, Q. Dong and J. Qiu, *Environ. Sci.- Nano*, 2019, **6**, 2379-2388.

S70 S. Wang, G. Wang, T. Wu, C. Li, Y. Wang, X. Pan, F. Zhan, Y. Zhang, S. Wang and J. Qiu, *Environ. Sci. Technol.*, 2019, **53**, 6292-6301.

S71 Z. Y. Leong and H. Y. Yang, *ACS Appl. Mater. Interfaces*, 2019, **11**, 13176-13184.

S72 T. Wu, G. Wang, S. Wang, F. Zhan, Y. Fu, H. Qiao and J. Qiu, *Environ. Sci. Tech. Let.*, 2018, **5**, 98-102.

S73 M. Li and H. G. Park, *ACS Appl. Mater. Interfaces*, 2018, **10**, 2442-2450.

S74 A. G. El-Deen, N. A. M. Barakat and H. Y. Kim, *Desalination*, 2014, **344**, 289-298.

S75 W. Cai, Z. Xiong, T. Hussain, J. Yang, Y. Wang and J. Liu, *J. Electrochem. Soc.*, 2016, **163**, A2515-A2523.

S76 Y. Liu, B. Geng, Y. Zhang, X. Gao, X. Du, X. Dou, H. Zhu and X. Yuan, *Desalination*, 2021, **504**, 114977.

S77 X. Gu, Y. Yang, Y. Hu, M. Hu and C. Wang, *ACS Sustain. Chem. Eng.*, 2015, **3**, 1056-1065.

S78 X. Gu, Y. Yang, Y. Hu, M. Hu, J. Huang and C. Wang, *J. Mater. Chem. A*, 2015, **3**, 5866-5874.

S79 J. Li, B. Hu, P. Nie, X. Shang, W. Jiang, K. Xu, J. Yang and J. Liu, *Appl. Surf. Sci.*, 2021, **542**, 148715.

S80 I. W. Siriwardane, N. P. W. Rathuwadu, D. Dahanayake, C. Sandaruwan, R. M. de Silva and K. M. N. de Silva, *Nanoscale Adv.*, 2021, **3**, 2585-2597.

S81 T. K. A. Nguyen, E. P. Kuncoro and R.-A. Doong, *Electrochim. Acta*, 2022, **401**, 139488.

S82 A. Therese Angeles, J. Park, K. Ham, S. Bong and J. Lee, *Sep. Purif. Technol.*, 2022, **280**, 119873.

S83 J. Lee, P. Srimuk, K. Aristizabal, C. Kim, S. Choudhury, Y. C. Nah, F. Mucklich and V. Presser, *ChemSusChem*, 2017, **10**, 3611-3623.

S84 B. Liu, L. Yu, F. Yu and J. Ma, *Desalination*, 2021, **500**.

S85 D. M. Sayed, M. S. El-Deab and N. K. Allam, *Sep. Purif.ication Technol.*, 2021, **266**.

S86 Z. Yue, Y. Ma, J. Zhang and H. Li, *J. Mater. Chem. A*, 2019, **7**, 16892-16901.

S87 X. Ma, Y.-A. Chen, K. Zhou, P.-C. Wu and C.-H. Hou, *Electrochim. Acta*, 2019, **295**, 769-777.

S88 W. Xi and H. Li, *Environ. Sci.- Wat. Res.*, 2020, **6**, 296-302.

S89 W. Xi and H. Li, *Environ. Sci.- Nano*, 2020, **7**, 764-772.

S90 M. Liang, X. Bai, F. Yu and J. Ma, *Nano Research*, 2020, **14**, 684-691.

S91 G. Wang, T. Yan, J. Shen, J. Zhang, L. Shi and D. Zhang, *Environ. Sci.- Nano*, 2021, **8**, 122-130.

S92 A. G. El-Deen, N. A. M. Barakat, K. A. Khalil, M. Motlak and H. Yong Kim, *Ceram. Int.*, 2014, **40**, 14627-14634.

S93 K. Xie, J. Yu, X. Zhang, S. Hu, R. Liu, H. Song, J. Shen, Y. Wang, A. Li and S. Zhang, *Chem. Eng. J.*, 2021, **414**, 128747.

S94 W. Wang, Z. Liu, Z. Zhang and H. Li, *Glob. Chall.*, 2022, **6**, 2100095.

S95 Y. Li, Y. Cai, Y. Wang, D. Liu and J. Guo, *J. Environ. Chem. Eng.*, 2022, **10**, 107266.

S96 A. S. Yasin, D. h. Kim and K. Lee, *J. Alloy. Compd.*, 2021, **870**, 159422.

S97 A. S. Yasin, A. Y. Mohamed, D. Kim, S. Yoon, H. Ra and K. Lee, *Micromachines*, 2021, **12**, 1148.

S98 E. Delfani, A. Khodabakhshi, S. Habibzadeh, L. Naji and M. R. Ganjali, *RSC Adv.*, 2022, **12**, 907-920.

S99 S. Vafakhah, M. Saeedikhani, S. Huang, D. Yan, Z. Y. Leong, Y. Wang, L. Hou, L. Guo, P. Valdivia y Alvarado and H. Y. Yang, *J. Mater. Chem. A*, 2021, **9**, 10758-10768.

S100 X. Wen, M. Zhao, M. Zhang, X. Fan and D. Zhang, *ACS Sustain. Chem. Eng.*, 2019, **8**, 1268-1275.

S101 Y. Wang, L. Zhang, Y. Wu, S. Xu and J. Wang, *Desalination*, 2014, **354**, 62-67.

S102 D. Ma, Y. Wang, X. Han, S. Xu and J. Wang, *Sep. Purif. Technol.*, 2018, **201**, 167-178.

S103 Y. Cai, Y. Wang, X. Han, L. Zhang, S. Xu and J. Wang, *J. Electroanal. Chem.*, 2016, **768**, 72-80.

S104 K. Xu, Y. Liu, Z. An, G. Xu, A. J. Gadgil and G. Ruan, *Desalination*, 2020, **486**, 114407.

S105 Y. Li, Z. Ding, J. Li, J. Li, T. Lu and L. Pan, *Desalination*, 2019, **469**, 114098.

S106 X. Xu, T. Yang, Q. Zhang, W. Xia, Z. Ding, K. Eid, A. M. Abdullah, M. Shahriar A. Hossain, S. Zhang, J. Tang, L. Pan and Y. Yamauchi, *Chem. Eng. J.*, 2020, **390**, 124493.

S107 D. Sriramulu and H. Y. Yang, *Nanoscale*, 2019, **11**, 5896.

S108 Y. Huang, F. Chen, L. Guo, H. Y. Yang, *J. Mater. Chem. A*, 2017, **5**, 18157.

S109 L. Guo, Y. Huang, M. Ding, Z. Y. Leong, S. Vafakhah and H. Y. Yang, *J. Mater. Chem. A*, 2018, 6, 8901.

S110 S. Vafakhah, L. Guo, D. Sriramulu, S. Huang, M. Saeedikhani and H. Y. Yang, *ACS Appl. Mater. Interfaces*, 2019, **11**, 5989.

S111 C. Hu, T. Wang, J. Dong, R. Liu, H. Liu, J. Qu, *Appl. Surf. Sci.*, 2018, **459**, 767.

S112 W. Shi, X. Liu, T. Deng, S. Huang, M. Ding, X. Miao, C. Zhu, Y. Zhu, W. Liu, F. Wu, C. Gao, S. Yang, H.Y. Yang, J. Shen, X. Cao, *Adv. Mater.*, 2020, **32**, 1907404.

S113 L. Guo, R. Mo, W. Shi, Y. Huang, Z. Y. Leong, M. Ding, F. Chen, H. Y. Yang, *Nanoscale*, 2017, **9**, 13305-13312.